IEEE Access
Multidisciplinary | Rapid Review | Open Access Journal

Received August 14, 2019, accepted August 31, 2019, date of publication September 5, 2019,
date of current version September 24, 2019.

Digital Object Identifier 10.1109/ACCESS.2019.2939546

Robust Fault Diagnosis of Rolling Bearings Using Multivariate Intrinsic Multiscale Entropy Analysis and Neural Network Under Varying Operating Conditions

RUI YUAN[1,2], YONG LV[1,2], HEWENXUAN LI[3], AND GANGBING SONG[4], (Member, IEEE)

[1]Key Laboratory of Metallurgical Equipment and Control Technology, Wuhan University of Science and Technology, Ministry of Education, Wuhan 430081, China
[2]Hubei Key Laboratory of Mechanical Transmission and Manufacturing Engineering, Wuhan University of Science and Technology, Wuhan 430081, China
[3]Department of Mechanical, Industrial and Systems Engineering, University of Rhode Island, Kingston, RI 02881, USA
[4]Smart Material and Structure Laboratory, Department of Mechanical Engineering, University of Houston, Houston, TX 77204, USA

Corresponding authors: Yong Lv (lvyong@wust.edu.cn) and Gangbing Song (gsong@uh.edu)

This work was supported by the National Natural Science Foundation of China under Grant 51875416 and Grant 51475339.

ABSTRACT olling bearings are crucial components in mechanical, civil and aerospace engineering. The practical working conditions of rolling bearings are complex and tough, hence fault diagnosis of rolling bearings under varying operating conditions is very challenging. This paper proposes a robust fault diagnosis approach of rolling bearings using multivariate intrinsic multiscale entropy analysis and neural network under varying operating conditions. The proposed approach deals with multivariate signal collected from multi-sensor acquisition system to capture much dynamical characteristic information. Multivariate intrinsic multiscale entropy analysis consists of adaptive projection intrinsically transformed multivariate empirical mode decomposition with adaptive noise (APIT-MEMD-AN) and improved multivariate multiscale sample entropy (IMMSE) with smoothed coarse graining process. Intrinsic mode functions (IMFs) obtained by APIT-MEMD-AN depict dynamical properties of multivariate signals. IMMSE of certain orders IMFs are adopted as input values of back propagation (BP) neural network to achieve fault classification of rolling bearings. APIT-MEMD-AN and IMMSE endow the proposed approach with the underlying adaptivity and robustness, making the proposed approach a fully data driven and robust method. Theoretical derivations, numerical simulations and experimental results verify the effectiveness and superiority of the proposed approach. The research work demonstrates the proposed approach is promising in fault diagnosis of rotary machinery under varying operating conditions.

INDEX TERMS Robust fault diagnosis, varying operating conditions, adaptive projection intrinsically transformed multivariate empirical mode decomposition with adaptive noise (APIT-MEMD-AN), improved multivariate multiscale sample entropy (IMMSE), smoothed coarse graining, neural network.

I. INTRODUCTION

Rolling bearings are crucial components in mechanical, civil and aerospace systems, and their working conditions have great influence on the entire system [1]–[3]. Practical working conditions of rolling bearings are usually complex and tough, and rolling bearings usually work under varying operating conditions, hence rolling bearings are prone to failure. Fault diagnosis of rolling bearings under varying operating conditions is very important but also challenging in practical applications. The signal processing methods, such as wavelet transform (WT) [4], [5], local mean decomposition (LMD) [6], [7] and variational mode decomposition (VMD) [8], [9], have been widely used in the field of fault diagnosis of rolling bearings. Apart from those methods, empirical mode decomposition (EMD) has drawn much attention in recent years [10]–[12]. It decomposes a nonlinear and nonstationary signal into approximate stationary

The associate editor coordinating the review of this manuscript and approving it for publication was Dong Wang.

time series representing time scales of the signal, denoting its frequency components. The obtained modes are intrinsic mode functions (IMFs), which are complete, adaptive and orthogonal expressions determined by signal itself instead of preset basis functions. IMFs arrange from high-to-low instantaneous frequencies. EMD was then extended to complex domain to deal with complex-valued data [13]. Complex EMD was proposed based on certain inherent properties of complex signals, including correlation between real and imaginary parts of complex signals [14]. Rotation invariant complex EMD was proposed afterwards by developing a consistent framework to process real and complex signals. The complex signal is decomposed in complex domain instead of being divided into two parts, which is achieved by employing complex splines to conduct all algorithms.

Compared with single sensor acquisition system, multi-sensor acquisition system collects more information, avoids data loss and eliminates uncertainty of information [15], [16]. Multi-channel signal improves the accuracy and reliability of obtained information to fully describe mechanical dynamic systems. As for multivariate signal processing, EMD needs to analyze each channel data separately, and data fusion is then conducted by weighting functions, resulting in different orders and inconsistent frequency scales among obtained multiple sets of IMFs. It may cause serious adverse effect in synchronous correlation analysis of multivariate signals. Hence, EMD reduces the effectiveness and accuracy of fault diagnosis of rotary machinery in processing multivariate signal. Bivariate empirical mode decomposition (BEMD) was proposed to process binary signal [17]–[19], whose local means are obtained by projecting in multiple directions. Then direction vectors are unevenly distributed on complex plane. The local extremums of projections are interpolated by using a complex-valued spline function, then local means are obtained by calculating envelop means. Afterwards, BEMD was further developed to trivariate empirical mode decomposition (TEMD) [20], treating trivariate signal as a pure quaternion, namely super complex. Each component is considered as a real value time series. After projecting trivariate signal in multiple directions in the middle of three dimensions, the extremums of projections are interpolated by a specific spline function to obtain a three-dimensional pure quaternion envelope curve. The local means of the trivariate signal are obtained by calculating the means of quaternion envelope curves.

BEMD and TEMD have been applied to bivariate and trivariate signal processing, however they are not applicable to multivariate signal processing. BEMD and TEMD cannot analyze multivariate signals under the premise of physical meaning and lack of theoretical basis. In the follow-up studies, EMD was extended to multivariate signal processing by proposing multivariate empirical mode decomposition (MEMD) [21]. The local means and envelopes are computed by real-valued projections on hyperspheres along multiple directions, hence MEMD perfectly solves mode alignment problem of IMFs. MEMD decomposes multivariate signal into multiple sets of IMFs, and the same characteristic frequencies appear in the same orders of different sets of IMFs. This property benefits for mode alignment according to frequency ranges across multiple channels. MEMD deals with multivariate signal collected by multiple sensors at different locations of mechanical systems. It has advantages of EMD processing nonlinear and nonstationary signals and successfully solves IMFs disorders among multiple channels. MEMD has been applied in simultaneous processing of multivariate signal in the fields of fault diagnosis of rotary machinery [22], [23], biomedical signal processing [24] and image processing [25]. Complete ensemble empirical mode decomposition with adaptive noise (CEEMDAN) [26], [27] was proposed by utilizing intrinsic filter bank property to solve the defect of generating different numbers of IMFs. Gaussian white noises are added into the signal to obtain one IMF in each iteration to avoid reconstruction error and ensure the same amounts of IMFs. Analogously, the property of MEMD in the presence of Gaussian white noise was studied [28], and it has been found that MEMD can act as a dyadic filter bank on each channel of the multivariate signal. The filter banks are used to incorporate down-sampling to reduce decomposed data in decimated MEMD filter banks [29]. The undecimated and decimated MEMD filter banks were studied [30], and the properties equip MEMD with down-sampling into any arbitrary tree structure and provide flexibility in the selection of frequency bands.

Due to the fast and wide developments of multi-sensor acquisition system, multivariate signal processing has drawn much attention. Since multiple sensors are placed at different locations on rotary machinery, power imbalances inevitably exist among multiple channels of the multivariate signal. It requires multivariate signal processing methods to alleviate adverse effect caused by power imbalances among multiple channels. Nonuniformly sampled bivariate empirical mode decomposition (NS-BEMD) [19], [31], nonuniformly sampled trivariate empirical mode decomposition (NS-TEMD) [32] were proposed to alleviate adverse effect power imbalances among bivariate and trivariate signal processing. Adaptive projection intrinsically transformed multivariate empirical mode decomposition (APIT-MEMD) [33] was afterwards proposed to deal with multivariate signals. APIT-MEMD mitigates mode-mixing problem by obtaining more accurate IMFs and alleviates adverse effect of power imbalances. The algorithm adopts the strategy to relocate n-dimensional uniform vectors on n-dimensional ellipsoid by finding the first principal component to conduct adaptive projections.

Approximate entropy [34] was proposed to measure the complexity and statistical quantification of time series and has been applied in physiological time series analysis. Afterwards, sample entropy (SE) was proposed [35], [36] as a refined version of approximate entropy, which obtains stable entropy values from short data and has proper anti-noise ability. SE compares the data in time series within itself as self-matching and measures new information of

the obtained time series, but it results in false information occasionally. Multiscale sample entropy (MSE) [37] was then proposed to analyze the complexity and regularity of time series on multiple scales, where coarse graining process is conducted to analyze multiscale time series at each scale. MSE better reflects dynamical characteristics of time series and greatly enrich the meaning of SE. The greater the probability of generating new patterns is, the more complex the time series is, and the larger entropy value is, and vice versa. MSE has been adopted as condition indicators in biomedical signal processing [38], [39] and fault diagnosis of rotary machinery [40], [41]. Multivariate multiscale sample entropy (MMSE) was proposed afterwards to compute MSE of multivariate signal and has been used to detect characteristic evolution of multivariate signals [42]–[45]. In the authors' previous studies [46], improved multivariate multiscale sample entropy (IMMSE) was proposed with introducing smoothed coarse graining process. IMMSE was adopted in health degradation monitoring of rotary machinery, and its effectiveness and superiority have been validated.

The adaptivity of APIT-MEMD in decomposition and the verified robustness of IMMSE in measuring the complexity and regularity of multivariate signals are very beneficial for fault diagnosis of rotary machinery. This paper proposes a novel robust fault diagnosis approach of rotary machinery under varying operating conditions, using multivariate intrinsic multiscale entropy analysis and neural network. Multivariate intrinsic multiscale entropy analysis consists of adaptive projection intrinsically transformed multivariate empirical mode decomposition with adaptive noise (APIT-MEMD-AN) and IMMSE. APIT-MEMD-AN can alleviate adverse effect of power imbalances among multiple channels of the collected multivariate signal and utilize its underlying filter bank property. IMMSE employs smoothed coarse graining process, and IMMSE values are used as condition indicators and taken as input values of back propagation (BP) neural network to achieve fault diagnosis of rolling bearings. The rest of the paper is as follows: Section II introduces the methodologies of APIT-MEMD-AN and IMMSE. Section III elaborates the proposed robust fault diagnosis approach of rolling bearings under varying operating conditions. Section IV presents numerical simulations of APIT-MEMD-AN and IMMSE, and comparative studies. Section V gives experimental verification, analysis and discussions. Section VI concludes the paper with major findings of research work, necessary discussions and future plans.

II. METHODOLOGIES

A. ADAPTIVE PROJECTION INTRINSICALLY TRANSFORMED MEMD WITH ADAPTIVE NOISE (APIT-MEMD-AN)

MEMD is the multivariate extension of EMD, and it can decompose a multivariate signal into multiple sets of IMFs, which are arranged in the order of high-to-low instantaneous frequencies [21]. Each IMF set has the same number of IMFs, and IMFs denoting the same frequencies locate in identical orders. The algorithm of MEMD has been elaborated in the authors' previous studies [47], [48]. To better illustrate the principle of APIT-MEMD, the principles of NS-BEMD [19], [31] and NS-TEMD [32] are introduced here. NS-BEMD algorithm adopts the elliptic statistical method to optimize BEMD algorithm by considering the relationship between the second order statistical structure and elliptic parameters of the bivariate signal represented by the circular quotient. The sampled vectors are mainly projected along the direction of principal component. It is important to determine direction vectors of the highest curvatures of the trivariate signal in three dimensions in NS-TEMD. Nonuniform samples may not align with the highest curvature directions to determine global nonuniformly sampled projections, which could result in suboptimal estimations of local means of the trivariate signal. Hence, a combination of uniformly and nonuniformly sampling strategies is employed. The highest curvature direction that is not captured by the nonuniform samples can be captured by uniform samples, and both samples can be adopted for the projections of the trivariate signal, thereby accurate local mean estimations can be performed.

For global nonuniform sampling strategy of the trivariate signal, the principal direction needs to be determined initially. The principal direction is determined based on the power imbalances and the correlation across multiple channels. For the trivariate signal $x(t)$, the covariance matrix is $\boldsymbol{C} = E\left\{x^T(t)\,x(t)\right\}$, where $E\{\cdot\}$ is the statistical expectation operator, and $(\cdot)^T$ is the transpose operator. The principal direction is obtained by eigenvalue decomposition of the covariance matrix $\boldsymbol{C} = \mathbf{V}\boldsymbol{\Lambda}\mathbf{V}^{\boldsymbol{T}}$. Elements on the diagonal matrix $\boldsymbol{\Lambda}$ correspond to eigenvalues, and the eigenvalue matrix $\mathbf{V}$ correspond to eigenvectors of the covariance matrix $\boldsymbol{C}$. The eigenvalue matrix characterizes the principal direction of $x(t)$, and eigenvalues characterize the relative power of the generated vectors.

To perform nonuniform sampling based on the statistical characteristics of the trivariate signal, an ellipsoid of a Cartesian coordinate system is generated as follows:

$$\begin{aligned} x &= a\cos\theta\sin\phi \\ y &= b\sin\theta\cos\phi \\ z &= c\cos\theta \end{aligned} \tag{1}$$

where θ is the tilt angle, ϕ is the azimuth angle, and a, b, c are the relevant parameters of the ellipsoid. The Hammersley sequence is adopted to uniformly sample the ellipsoid and determine the azimuth angle ϕ_H and the tilt angle θ_H. The Hammersley projection is used to determine the coordinate system of the uniformly sampled sphere, so that the ellipsoid is sampled along the direction of the largest curvature.

As for multivariate signals, APIT-MEMD basically adopts analogous strategy which relocates n-dimensional uniform vectors on n-dimensional ellipsoid. In APIT-MEMD, the first principal component adaptively denotes the direction of maximum power imbalance and determines the correlation

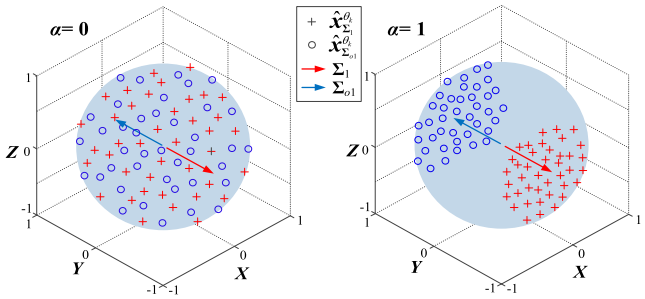

FIGURE 1. Adaptive projection vectors by adopting the proposed strategy ($\alpha = 0, 1$).

across multiple channels. For multivariate signal $x(t)$, its covariance matrix is $\boldsymbol{C} = E\left\{x^T(t)\,x(t)\right\}$, where $E\{\cdot\}$ and $(\cdot)^T$ denote statistical expectation operator and transpose operator, respectively. The first principal component direction is determined by eigenvalue decomposition of the covariance matrix $\boldsymbol{C} = \boldsymbol{\Sigma\Lambda\Sigma^T}$, where $\boldsymbol{\Sigma} = [\Sigma_1, \Sigma_2, \cdots, \Sigma_n]$ denotes the eigenvector matrix, and all values on the diagonal matrix $\boldsymbol{\Lambda} = \mathrm{diag}\{\boldsymbol{\lambda_1}, \boldsymbol{\lambda_2}, \cdots, \boldsymbol{\lambda_n}\}$ are eigenvalues of the covariance matrix $\boldsymbol{C}$. The largest eigenvalue λ_1 of $\boldsymbol{\Lambda}$ corresponds to eigenvector Σ_1 of the first principal component direction which characterizes maximum power imbalance. $\boldsymbol{\Sigma}_1$ is used to construct another vector $\boldsymbol{\Sigma}_{o1}$ which is along its opposite direction, $\boldsymbol{\Sigma}_{o1} = -\boldsymbol{\Sigma}_1$. Then $\boldsymbol{\Sigma}_1$ and $\boldsymbol{\Sigma}_{o1}$ are used to reset the direction vectors obtained from uniform projection strategy. During the iteration process, $x(t)$ is iterated along these adaptive projection vectors, and local means are obtained by MEMD. APIT-MEMD alleviates adverse effect of power imbalances among multiple channels by large amounts of adaptive projection vectors. The adaptive projection strategy is illustrated in Fig. 1, where $\alpha = 0$ denotes that there are no considerable power imbalances, while $\alpha = 1$ denote high power imbalances among multiple channels.

Furthermore, to utilize the filter bank property of APIT-MEMD in the presence of Gaussian white noise, the key idea of CEEMDAN [26], [27] is adopted here. APIT-MEMD-AN is proposed in this paper. The main steps of APIT-MEMD-AN are as follows:

1) Add n_2 channels Gaussian white noise to original n_1 channels multivariate signal $x(t)$ to form the multivariate signal $s(t)$ in each iteration. The Gaussian white noise is $\varepsilon_k \mathrm{std}(r_k)$, where ε_k is usually set as 0.02 and r_k is the signal to be decomposed in each iteration. In first iteration, $r_k = x(t)$. In the subsequent iterations, r_k denotes the signal after subtracting the obtained IMF, thus only one IMF set is generated in each iteration.
2) Perform eigenvalue decomposition of the covariance matrix of the multivariate signal $s(t)$, $\boldsymbol{C} = \boldsymbol{\Sigma\Lambda\Sigma^T}$, where $\boldsymbol{\Sigma}$ is the eigenvector matrix, $\boldsymbol{\Lambda}$ is the eigenvalue matrix. The largest eigenvalue λ_1 corresponds to eigenvector Σ_1, namely first principal component denotes the direction of maximum power imbalance. Then construct another vector Σ_{o1} along the opposite direction of Σ_1.
3) Adopt Hammersley sequence to uniformly sample on the $(n-1)$ dimensional sphere to obtain K uniform projection vectors $\left\{\boldsymbol{x}^{\theta_k}\right\}_{k=1}^{K}$. Afterwards, calculate Euclidean distance between each direction vector and Σ_1.
4) Reset uniform projection vectors $\boldsymbol{x}_{\boldsymbol{\Sigma}_1}^{\theta_k}$ on the half ellipsoid where Σ_1 is located, according to:

$$\hat{\boldsymbol{x}}_{\boldsymbol{\Sigma}_1}^{\theta_k} = \frac{\boldsymbol{x}_{\boldsymbol{\Sigma}_1}^{\theta_k} + \alpha\boldsymbol{\Sigma}_1}{\left|\boldsymbol{x}_{\boldsymbol{\Sigma}_1}^{\theta_k} + \alpha\boldsymbol{\Sigma}_1\right|} \tag{2}$$

Reset uniform projection vectors $\boldsymbol{x}_{\boldsymbol{\Sigma}_{o1}}^{\theta_k}$ on another half of ellipsoid where Σ_{o1} is located, according to:

$$\hat{\boldsymbol{x}}_{\boldsymbol{\Sigma}_{o1}}^{\theta_k} = \frac{\boldsymbol{x}_{\boldsymbol{\Sigma}_{o1}}^{\theta_k} + \alpha\boldsymbol{\Sigma}_{o1}}{\left|\boldsymbol{x}_{\boldsymbol{\Sigma}_{o1}}^{\theta_k} + \alpha\boldsymbol{\Sigma}_{o1}\right|} \tag{3}$$

where α is determined by the degree of power imbalances among multiple channels of the multivariate signal.
5) Use adaptive projection direction vectors $\boldsymbol{x}_{\boldsymbol{\Sigma}_1}^{\theta_k}$ and $\boldsymbol{x}_{\boldsymbol{\Sigma}_{o1}}^{\theta_k}$ to conduct iterative decomposition, and local mean estimation is achieved based on MEMD, then obtain $(n_1 + n_2)$ sets of IMFs of $s(t)$.
6) Discard n_2 sets of IMFs, corresponding to added Gaussian white noise, from the resulting $(n_1 + n_2)$ sets of IMFs. Then n_1 sets of IMFs of $x(t)$ are obtained.

MEMD-derived methods solve mode alignment problem across multiple channels, which is beneficial for synchronous correlation analysis and has been illustrated in the author's previous studies [47], [48]. Multivariate signals are decomposed into multiple sets of IMFs arranging from high-to-low instantaneous frequencies adaptively. Multiple sets of IMFs are aligned to the same frequency ranges, and the same characteristics frequencies locate in the same orders of IMF sets. In addition, APIT-MEMD and APIT-MEMD-AN alleviate adverse effect of power imbalances among multiple channels by large amounts of adaptive projection vectors. Based on theoretical derivations, the advantages of APIT-MEMD-AN against APIT-MEMD in fault diagnosis of rotary machinery lie in two aspects as follows:

1) APIT-MEMD-AN utilizes the intrinsic filter bank property in the presence of Gaussian white noise with frequency uniformly distribution property to alleviate mode mixing problem. The extra noise channels serve as references to enable more stable and accurate IMFs depicting dynamical characteristic information.
2) By adding specific noise to each residue in each iteration of APIT-MEMD-AN, one IMF set is obtained each time, thus the same amounts of IMFs are generated under different ensemble times, which benefits for subsequent analysis of adopting certain orders IMFs. If different orders IMFs were generated in different decompositions, then it could cause confusion if certain orders IMFs were adopted in subsequent analysis.

B. IMPROVED MULTIVARIATE MULTISCALE SAMPLE ENTROPY (IMMSE)

MMSE was proposed based on MSE which was elaborated in the authors' previous studies [46]. MMSE algorithm is given here directly. Coarse graining process of p-variate time series $\{x_{k,i}\}_{i=1}^{N}$ is conducted for scale factor φ, where $k = 1, 2, \cdots, p$, $i = 1, 2, \cdots, N$, N is the number of points. The coarse-grained multivariate time series is obtained as follows:

$$y_{k,j}^{\varphi} = \frac{1}{\varphi} \sum_{i=(j-1)\varphi+1}^{j\varphi} x_{k,i} \tag{4}$$

where $1 \leq j \leq N/\varphi$. Then, calculate multivariate sample entropy (Multi-SE) of each coarse-grained multivariate $y_{k,j}^{\varphi}$, and plot Multi-SE as a function of the scale factor φ, namely MMSE. The main steps of Multi-SE are as follows:

1) The multivariate embedded reconstruction of a p-variate time series $\{x_{k,i}\}_{i=1}^{N}$ is based on composite delay vectors:

$$\begin{aligned} \boldsymbol{X}_m(i) = [&x_{1,i}, x_{1,i+\tau_1}, \cdots, x_{1,i+(m_1-1)\tau_1}, x_{2,i}, x_{2,i+\tau_2}, \\ &\cdots, x_{2,i+(m_2-1)\tau_2}, \cdots x_{p,i}, \\ &x_{p,i+\tau_p}, \cdots, x_{p,i+(m_p-1)\tau_p}] \end{aligned} \tag{5}$$

where $\boldsymbol{M} = [m_1, m_2, \cdots, m_p]$ and $\boldsymbol{\tau} = [\tau_1, \tau_2, \cdots, \tau_p]$ are the embedded vector and the time delay vector, respectively, in multivariate embedding reconstruction [49], [50].

2) Define the distance between any two vectors $\boldsymbol{X}_m(i)$ and $\boldsymbol{X}_m(j)$ as maximum criterion:

$$\begin{aligned} &D[\mathrm{X}_m(i), \mathrm{X}_m(j)] \\ &\quad = \max_{l=1,2,\cdots,m} \{|x(i+l-1) - x(j+l-1)|\} \end{aligned} \tag{6}$$

3) Determine the number of vector pair of the composite delay vector $\boldsymbol{X}_m(i)$ as P_i and threshold is r. $D[\boldsymbol{X}_m(i), \boldsymbol{X}_m(j)] \leq r$. The occurrence frequency $B_i^m(r) = P_i/(N-n-1)$, and $n = \max\{\boldsymbol{M}\} \times \max\{\boldsymbol{\tau}\}$.

4) Compute the average of all $B_i^m(r)$:

$$B^m(r) = \frac{1}{N-n} \sum_{i=1}^{N-n} B_i^m(r) \tag{7}$$

5) Extend the multivariate delay vector to $m+1$, and other data channels remain unchanged, so the general embedding dimension of multivariate time series increases to $m+1$.

6) Repeat steps of (2)-(5) to calculate all $B_i^{m_k+1}(r)$ and mean value $B_i^{m+1}(r)$ upon k, then its mean value $B^{m+1}(r)$ upon i is denoted as:

$$B^{m+1}(r) = \frac{1}{p(N-n)} \sum_{i=1}^{p(N-n)} B_i^{m+1}(r) \tag{8}$$

where $B^m(r)$ denotes the possibility of similarity of any two composite delay vectors in m dimensional phase space.

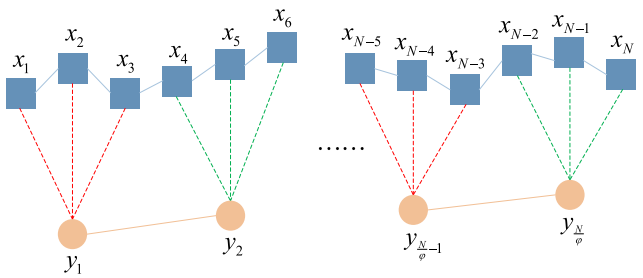

FIGURE 2. Illustration of traditional coarse graining process.

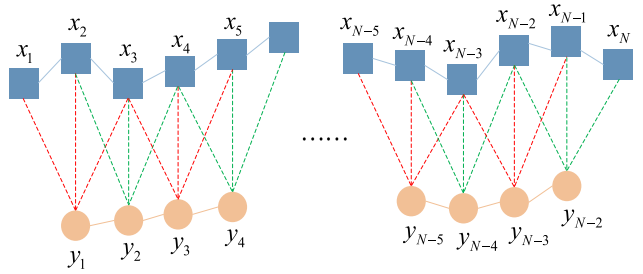

FIGURE 3. Illustration of the proposed smoothed coarse graining process.

7) Multi-SE can be denoted as:

$$\text{Multi-SE}(\mathrm{M}, \boldsymbol{\tau}, r, N) = \mathrm{In}B^m(r) - \mathrm{In}B^{m+1}(r) \tag{9}$$

During the coarse graining process, when scale factor $\varphi = 3$, traditional coarse graining process is illustrated in Fig. 2. Fig. 2 shows that the time series is compressed by traditional coarse graining process according to scale factor. When the scale increases, the length of coarse-grained time series decreases, hence traditional coarse graining process cannot guarantee the same length of coarse-grained time series. When the length of the time series is not an integer multiple of scale factor, there will be data loss during coarse graining process. These two main drawbacks inevitably affect the accuracy and effectiveness of MMSE algorithm. To solve these drawbacks, IMMSE was proposed by using proposed smoothed coarse graining process in the authors' previous studies [46], which adopts a sliding average during coarse graining process. When scale factor $\varphi = 3$, the proposed smoothed coarse graining process is illustrated in Fig. 3, which guarantees the same length of coarse-grained time series and avoids data loss.

III. THE PROPOSED FAULT DIAGNOSIS OF ROLLING BEARINGS BASED ON MULTIVARIATE INTRINSIC MULTISCALE ENTROPY ANALYSIS UNDER VARYING OPERATING CONDITIONS

When different kinds of faults occur to rolling bearings, the complexities of structural dynamical responses are different. Recognition of structural dynamical responses achieves fault diagnosis of rolling bearings. Studies on EMD-derived methods indicate that IMFs depict signal dynamics and

the underlying properties of decoupling frequency information [51]–[55]. Using multiple sensors to collect multivariate signals avoids the loss of local information and ensures to capture maximum dynamical information. The filter bank property of APIT-MEMD is studied in this paper, and APIT-MEMD-AN is proposed to process multivariate signals of rolling bearings. The IMFs depict intrinsic dynamical properties of multivariate vibration signals of different kinds of faulty rolling bearings. Certain orders IMFs can be used to extract fault characteristic information. Since IMMSE values measure the complexity and regularity of vibration signals. Here, IMMSE values are adopted as condition indicators to measure the complexity and regularity of multivariate vibration signals of rotary machinery under varying operating conditions [46].

This paper proposes a novel robust fault diagnosis approach of rolling bearings under varying operating conditions using multivariate intrinsic multiscale entropy analysis and neural network. Multivariate intrinsic multiscale entropy analysis consists of APIT-MEMD-AN and IMMSE. APIT-MEMD-AN decomposes multivariate signals into multiple sets of IMFs, arranging from high-to-low instantaneous frequencies. Certain orders IMFs are selected and used to depict dynamical properties of multivariate vibration signals. IMMSE of certain orders IMFs are taken as condition indicators and adopted as input values of BP neural network to achieve fault diagnosis of rolling bearings. IMMSE measures the complexity of multivariate vibration signals, instead of energy or frequency amplitudes. Different kinds of faulty rolling bearings are classified by intrinsic dynamical properties. Hence the results of the proposed fault diagnosis approach won't be affected by varying operating conditions. BP neural network is a multi-layer feedforward neural network, with advantages of forward propagation of signals and backward propagation of errors. When output values differ from expected values, it would start to propagate backwards and optimize its topology and network weight by self-learning and self-adjustment [56], [57]. BP neural network can serve as a nonlinear function, where the input values A_n are condition indicators, and the predicted output values C_n are dependent variables. The topology of BP neural network is shown in Fig. 4. The output values C_1, C_2 and C_3 denote three kinds of defect types, which are inner race, ball and outer race defects, respectively. The schematic diagram of the proposed approach in this paper is illustrated in Fig. 5.

IV. NUMERICAL SIMULATIONS

To validate the effectiveness and superiorities of the proposed APIT-MEMD-AN and IMMSE, numerical simulations are given here. The same simulated multivariate signal is adopted in simulation researches of APIT-MEMD-AN and IMMSE for the consistency of numerical simulations, due to the strategy of multivariate intrinsic multiscale entropy analysis. Under practical conditions, apart from fault characteristic frequency of faulty rolling bearing, there are also structural intrinsic frequencies and modulation frequencies. Hence,

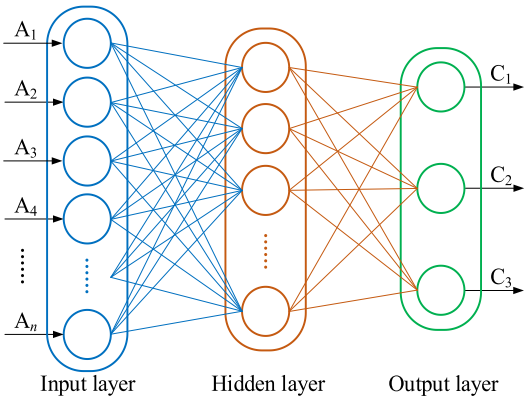

FIGURE 4. Illustration of BP neural network topology.

different frequency components are adopted to construct the simulated multivariate signal. Three original signals are given as follows:

$$\begin{aligned} x_1(t) &= \cos(2\pi f_1 t)\,[1 + \sin(2\pi f_2 t)] \\ x_2(t) &= \sin(2\pi f_3 t) \\ x_3(t) &= \sin(2\pi f_4 t)\,[1 + \cos(2\pi f_5 t)] \end{aligned} \tag{10}$$

where f_1, f_2, f_3, f_4, f_5 are 50 Hz, 10 Hz, 90 Hz, 140 Hz, 20 Hz, respectively. The sampling frequency is 4096 Hz, and the sampling point is 4096. Under practical conditions, three original signals are collected by each sensor simultaneously in multi-sensor acquisition system of rolling bearing. Simulated collected multivariate signal amplitudes are set as 1, 2 and 4 for 1st, 2nd and 3rd channels, respectively, to simulate power imbalances among multiple channels of multivariate signal. s denotes background noise, simulated by Gaussian white noise with variance of 0.4 and mean of 0. The simulated collected multivariate signal is given as follows:

$$\begin{aligned} S_1(t) &= x_1(t) + x_2(t) + x_3(t) + s \\ S_2(t) &= 2x_1(t) + 2x_2(t) + 2x_3(t) + 2s \\ S_3(t) &= 4x_1(t) + 4x_2(t) + 4x_3(t) + 4s \end{aligned} \tag{11}$$

A. SIMULATION RESEARCH OF APIT-MEMD-AN

APIT-MEMD-AN is proposed here by adopting its filter bank property in the presence of Gaussian white noise, and specific noise is added to each residue in each iteration during the decomposition to generate one IMF set each time. To verify the effectiveness and superiority of APIT-MEMD-AN over APIT-MEMD, numerical simulations are conducted here. The α is determined by the degree of power imbalances among three channels signal in APIT-MEMD-AN. The α values of 0 and 1 respectively denote the case without power imbalances and the case with high power imbalance. Under practical conditions, power imbalances inevitably exist among multiple channels of the multivariate signal, however its degree is hard to define. Hence, α is set as 0.5 to capture direction of highest power imbalance as a compromising solution. Two channels Gaussian white noise are added to

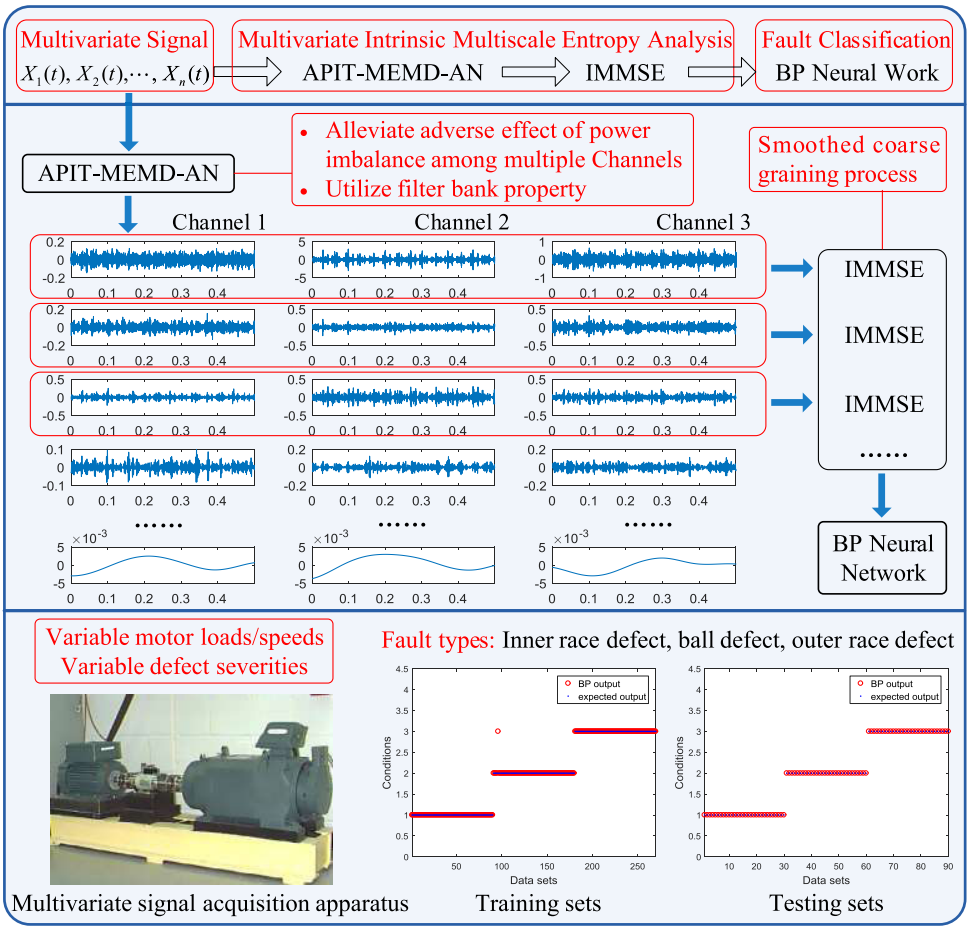

FIGURE 5. The schematic diagram of the proposed robust fault diagnosis approach using multivariate intrinsic multiscale entropy analysis and neural network under varying operating conditions.

multivariate signal to adopt its filter bank property, with variance of 0.4 and average of 0. In APIT-MEMD-AN, two channels Gaussian white noise are added to the signal in each iteration. In the first iteration of APIT-MEMD-AN, r_k denotes the simulated multivariate signal. In subsequent iterations, r_k denotes multivariate signal after subtracting one IMF set. Time domain plots of IMFs obtained by APIT-MEMD and APIT-MEMD-AN of the multivariate signal are shown in Fig. 6 and Fig. 7, respectively.

Fig. 6 and Fig. 7 show that 8 orders IMFs are obtained by APIT-MEMD, and 8 orders IMFs are obtained by APIT-MEMD-AN. The residue of the decomposition is not shown in each figure. From time domain plots of IMFs obtained by APIT-MEMD and APIT-MEMD-AN, it can be seen that the same characteristic frequencies locate in the same orders of IMFs with different amplitudes. To measure the superiority of APIT-MEMD-AN over APIT-MEMD in alleviating mode mixing problem to extract characteristic frequencies of the simulated multivariate signal, fault correlation factor (FCF) analysis [47] is conducted to determine effective IMFs. During FCF analysis, the 3rd, 4th and 5th orders IMFs obtained by APIT-MEMD are determined as effective, and frequency domain plots of effective IMFs are shown in Fig. 8. The 2nd, 3rd and 4th orders IMFs obtained by APIT-MEMD-AN are determined as effective, and frequency domain plots of effective IMFs are shown in Fig. 9.

It can be seen from Fig. 8 that in effective IMFs obtained by APIT-MEMD, characteristic frequencies f_4 and $f_4 \pm f_5$ of $x_3(t)$ appear in the 3rd order IMFs, characteristic frequency f_3 of $x_2(t)$ appears in the 3rd and 4th orders IMFs, and characteristic frequencies f_1 and $f_1 \pm f_2$ of $x_1(t)$ appear in the 4th and 5th orders IMFs. The analysis shows that there are mode mixing problems existing in IMFs obtained by APIT-MEMD. While Fig. 9 shows that in effective IMFs obtained by APIT-MEMD-AN, characteristic frequencies f_4 and $f_4 \pm f_5$ of $x_3(t)$ appear in the 2nd order IMFs, characteristic frequency f_3 of $x_2(t)$ appears in the 3rd order IMFs, and characteristic frequencies f_1 and $f_1 \pm f_2$ of $x_1(t)$ appear in the 4th order IMFs. The frequency analysis indicates that there is no mode mixing problem existing in IMFs obtained by APIT-MEMD-AN. Different characteristic frequencies locate exactly in different orders IMFs obtained by APIT-MEMD-AN. Further, it can be seen from Fig. 8 and Fig. 9 that IMFs obtained by APIT-MEMD-AN show less

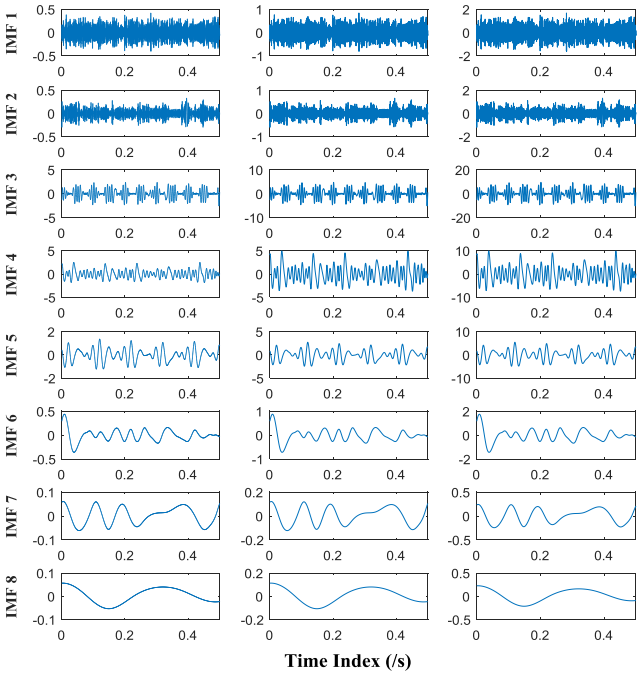

FIGURE 6. Time domain plots of IMFs obtained by APIT-MEMD of the multivariate signal.

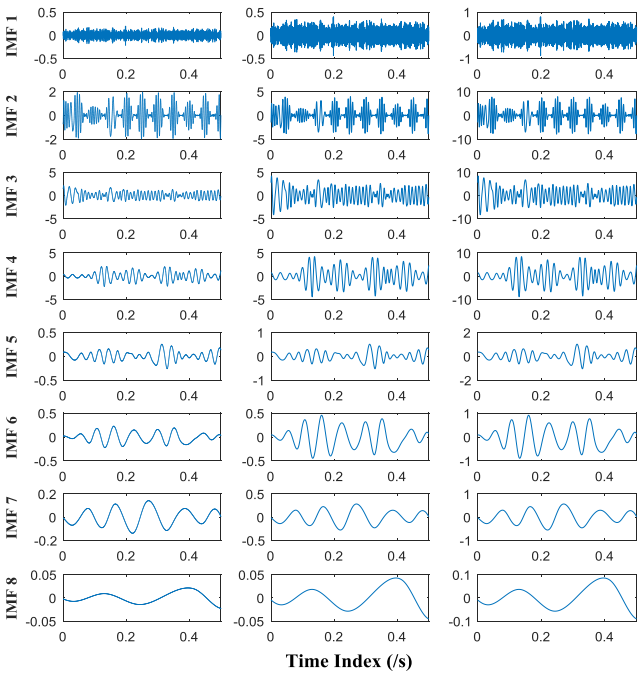

FIGURE 7. Time domain plots of IMFs obtained by APIT-MEMD-AN of the multivariate signal.

redundant noise frequency components, and more accurate characteristic frequency components than IMFs obtained by APIT-MEMD.

The comparative analysis of frequency domain plots shows that characteristic frequencies of multivariate signal can be extracted in IMFs obtained by APIT-MEMD and APIT-MEMD-AN, meaning adverse effect of power

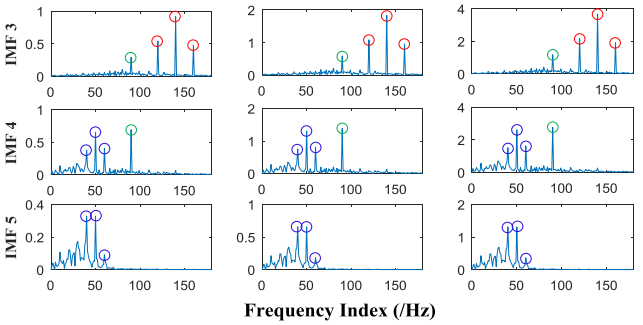

FIGURE 8. Frequency domain plots of effective IMFs obtained by APIT-MEMD, where red circles denote f_4 and its side frequencies $f_4 \pm f_5$, green circles denote f_3, and blue circles denote f_1 and its side frequencies $f_1 \pm f_2$.

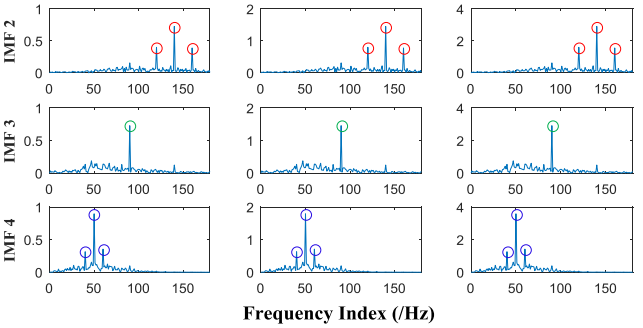

FIGURE 9. Frequency domain plots of effective IMFs obtained by APIT-MEMD-AN, where red circles denote f_4 and its side frequencies $f_4 \pm f_5$, green circles denote f_3, and blue circles denote f_1 and its side frequencies $f_1 \pm f_2$.

imbalances is alleviated. In addition, APIT-MEMD-AN shows superiority over APIT-MEMD in alleviating mode mixing problem to generate more accurate IMFs depicting dynamical properties of multivariate signal. Hence, from the above simulation research and comparative analysis, advantages of APIT-MEMD-AN against APIT-MEMD have been validated.

B. SIMULATION RESEARCH OF IMMSE

To verify the effectiveness and superiority of IMMSE over MMSE, numerical simulation and comparisons are given here. MMSE is improved by smoothed coarse graining process. For consistency of numerical simulations, due to the strategy of multivariate intrinsic multiscale entropy analysis, IMMSE and MMSE of the simulated multivariate signal in Equation (11) are computed here. Embedding dimension m and delay time τ are set as 5 and 1, respectively. Based on theoretical derivation in methodologies, a larger scale factor leads to clearer presentation of signal's complexity, however results in more computational load, meaning less computation efficiency. Taking presentation of signal's complexity and computation efficiency into account, the scale factor φ is selected as 20 in simulation research of IMMSE after several experimental trials.

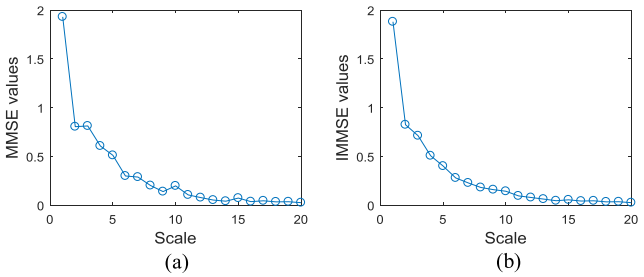

FIGURE 10. 1st experimental trial using 1 to 2048 points of multivariate signal: (a) MMSE values, (b) IMMSE values.

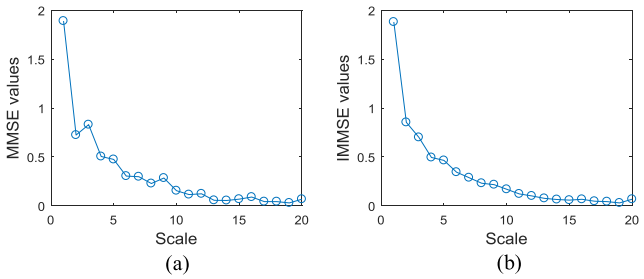

FIGURE 11. 2nd experimental trial using 2049 to 4096 points of multivariate signal: (a) MMSE values, (b) IMMSE values.

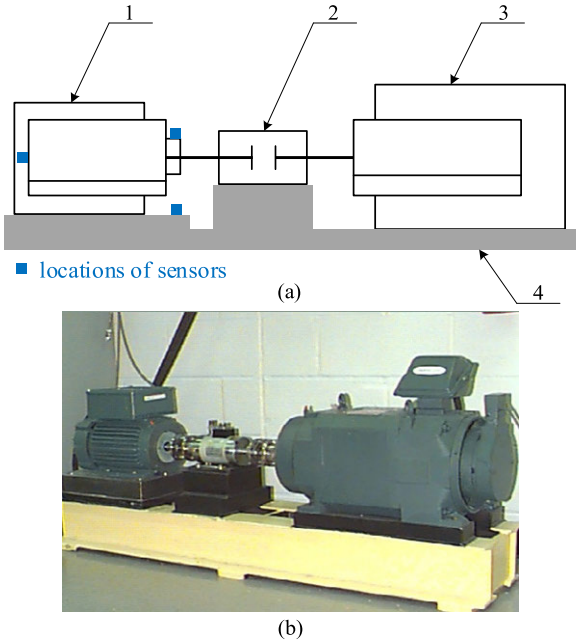

FIGURE 12. (a) The schematic of experimental apparatus,1-Motor, 2-Torque transducer/encoder, 3-Dynamometer, 4-Base plate. (b) A picture of experimental apparatus.

To validate the effectiveness and superiority of IMMSE over MMSE, multivariate signals from different starting points are analyzed. The length of the original multivariate signal is 4096, and multivariate signals with the length of 2048 points are adopted in two experimental trials, from 1 to 2048 (1st trial) and 2049 to 4096 (2nd trial), respectively. MMSE and IMMSE values of two experimental trials are shown in Fig. 10 and Fig. 11, respectively.

It can be seen from Fig. 10 and Fig. 11 that MMSE and IMMSE values of multivariate signal monotonically decrease. MMSE values, adopting traditional coarse graining process, show fluctuations along with the increase of scale factor. It can be seen from Fig. 10 (a) and Fig. 11 (a) that when scale factors are 2 and 3, MMSE values show fluctuations in overall variation trend. In Fig. 10 (a), when scale factors are 10 and 15, and in Fig. 11 (a), when scale factors are 9 and 16, MMSE values show fluctuations in overall variation trend. While IMMSE values, adopting smoothed coarse graining process, show robustness with the increase of scale factor in Fig. 10 (b) and Fig. 11 (b). The comparative analysis shows that IMMSE achieves more stable entropy values on multiple scales to reflect the complexity and regularity of multivariate signals. In addition, the comparisons between MMSE and IMMSE in two experimental trials verify the superiority of the proposed IMMSE over MMSE in reflecting the complexity and regularity of multivariate signals. Smoothed coarse graining process alleviates adverse effect of background noise. Hence, IMMSE can be applied in the field of fault diagnosis of rolling bearings.

V. EXPERIMENTAL VERIFICATION

The theoretical derivations and numerical simulations indicate that the proposed approach can be applied to fault diagnosis of rotary machinery. To validate the effectiveness and superiority of the proposed approach, practical experiments need to be conducted. Considering the authority of data sets used for practical experiments, faulty bearing data from *Case Western Reserve University Bearing Database* are used to verify the superiority of the proposed approach [58]. 6205-2RS JEM SKF rolling bearings were used in experiments. The electro discharge machining is adopted to cause defects on different parts of rolling bearing, to generate different types of faulty rolling bearings, including inner race, ball and outer race defects of rolling bearings. Three sensors were placed at different locations of the experimental apparatus, at the 12 o'clock positions of drive and fan ends of the motor housing, and motor supporting base plate. The sampling frequency in signal acquisition is 12 kHz. The schematic diagram of the experimental apparatus and a picture are shown in Fig. 12.

Faulty rolling bearings of different severities were used in the experiment, including defect diameters of 0.007, 0.014, and 0.021 inch. Motor loads are 0, 1, 2, 3 Hp and motor speeds are 1730, 1750, 1772, 1797 rpm. Rolling bearing of each kind of severity has 4 operating conditions, namely there are 12 operating conditions of faulty rolling bearings, which denotes varying operating conditions in this paper. To verify the validity and superiority of the proposed robust fault diagnosis approach of rotary machinery under varying operating conditions, the data sets of defect diameters of 0.007, 0.014 and 0.021 inch are both chosen to be analyzed to extract

TABLE 1. Illustrations of faulty rolling bearing data sets under varying operating conditions.

Defect diameter (inch)	Motor Operating conditions		Defect type (Data/8192 points)		
	Load (Hp)	Speed (rpm)	Inner race	Ball	Outer race
0.007"	0	1797	10	10	10
	1	1772	10	10	10
	2	1750	10	10	10
	3	1730	10	10	10
0.014"	0	1797	10	10	10
	1	1772	10	10	10
	2	1750	10	10	10
	3	1730	10	10	10
0.021"	0	1797	10	10	10
	1	1772	10	10	10
	2	1750	10	10	10
	3	1730	10	10	10

indicators for training sets and testing sets. For 12 operating patterns, 10 samples with the length of 8192 points of each defect are acquired from collected vibration signals. To achieve fault diagnosis of rolling bearings under varying operating conditions, 90 samples are randomly selected as training sets, and the remaining 30 samples are testing sets. The analyzed faulty rolling bearing data sets under varying operating conditions are illustrated in Table 1.

APIT-MEMD-AN is conducted to decompose one set multivariate signal of faulty rolling bearing, and time domain plots of the generated IMFs are shown in Fig. 13.

It can be seen from Fig. 13 that 11 orders IMFs are generated by APIT-MEMD-AN, and the residue of the decomposition is not shown in the figure. It should be noted that the effectiveness of the proposed method using different orders IMFs are different. Then IMMSE values of certain orders IMFs are computed and adopted as input values of BP neural network. IMMSE of one order IMFs are computed as a trial and shown in Fig. 14.

Fig. 14 shows that IMMSE values monotonically decrease along with the increase of scale factor. It has been illustrated in the authors' previous studies [46] that if IMMSE values of a multivariate signal monotonically decrease, and it means the multivariate signal has low self-similarity and contains most information at the smallest scale. Hence, IMMSE value of smallest scale is adopted as the condition indicator during fault diagnosis of rolling bearings.

The parameters of BP neural network are given as follows, and it has 2 hidden layers, apart from input and output layers. The detailed structure of BP neural network adopted in this paper, including training and learning function settings, and numbers of layers and neurons, is given in Table 2. The number of input neurons are selected as 7 denoting IMMSE values of 7 orders IMFs are computed and adopted as input of BP neural network, which will be illustrated hereinafter. The output layer has 3 neurons, denoting three defect types of rolling bearings. The training iterations, namely training times, is taken as 1000. The output neurons of BP neural network are shown in Table 3.

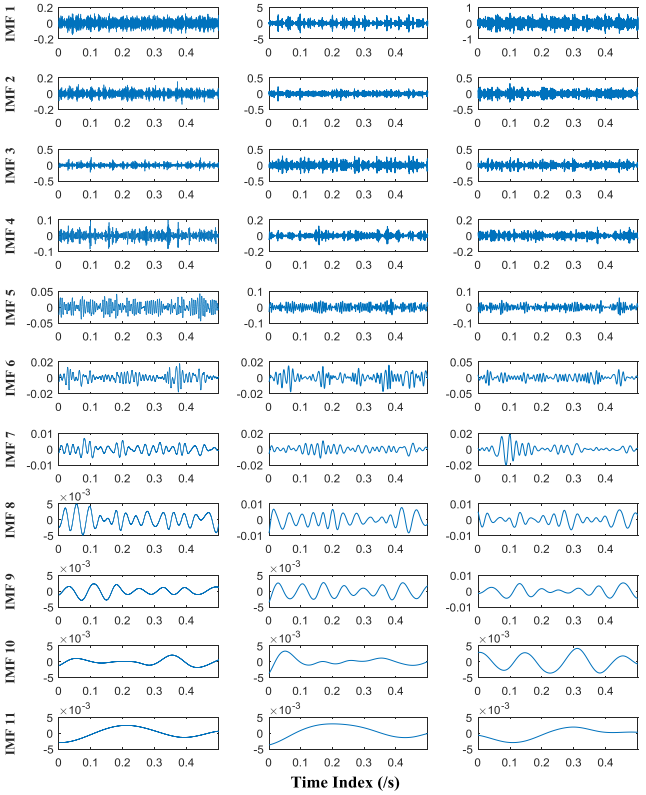

FIGURE 13. Time domain plots of IMFs obtained by APIT-MEMD-AN of multivariate signal.

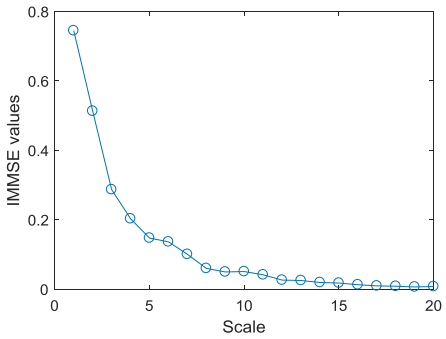

FIGURE 14. IMMSE values of one order IMFs adopting smoothed coarse graining process.

TABLE 2. The detailed structure of BP neural network.

Functions		Layer neurons		
		Input	Hidden (2)	Output
Trainlm	Learngdm	7	25	3

To verify the superiority of multivariate signal processing over single channel signal processing, the results of neural network adopting SE of the first 7 orders IMFs obtained by EMD, are shown in Fig. 15. The abscissas of Fig. 15 denote the data sets, and the ordinates 1, 2, 3 denote inner race, ball and outer race defects, respectively, based on the setting of

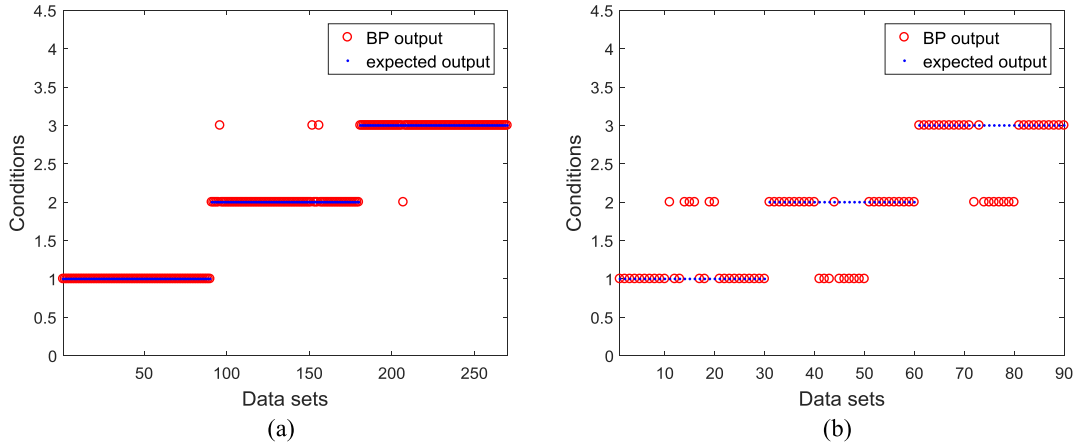

FIGURE 15. BP neural network results by utilizing 7 orders IMFs of EMD and SE: (a) Training sets, (b) Testing sets.

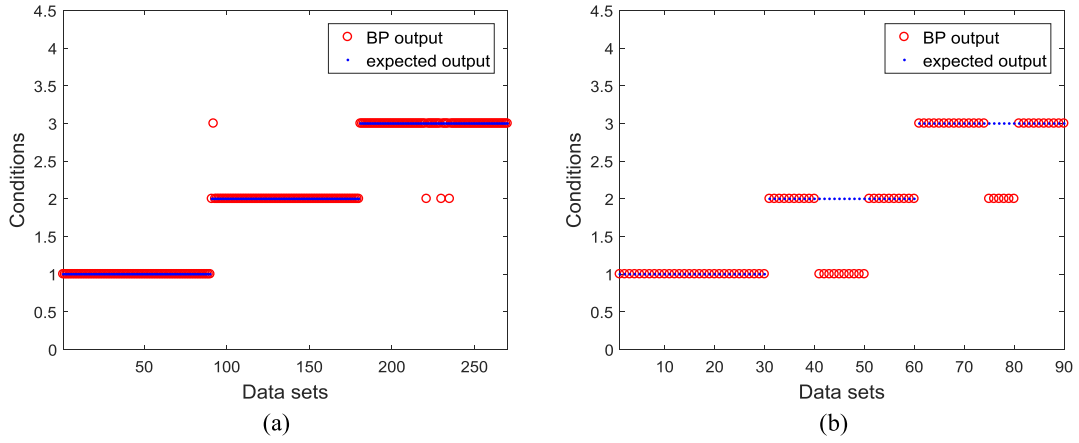

FIGURE 16. BP neural network results by utilizing 4 orders IMFs of APIT-MEMD-AN and IMMSE: (a) Training sets, (b) Testing sets.

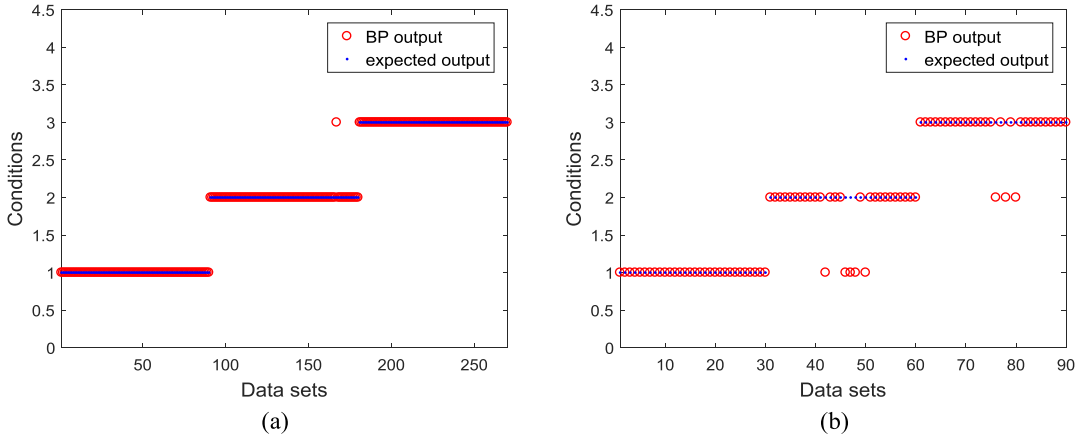

FIGURE 17. BP neural network results by utilizing 7 orders IMFs of MEMD and IMMSE: (a) Training sets, (b) Testing sets.

the output layer neurons in Table 3, and the same applies hereinafter.

Fig. 15 shows that fault classification accuracies in testing sets of BP neural network is far from good. Fault classification accuracies of inner race, ball, and outer race defects of rolling bearings in testing process of BP neural network are 80%, 70% and 76.67%. The results infer that SE of IMFs obtained by EMD of single-channel signal cannot

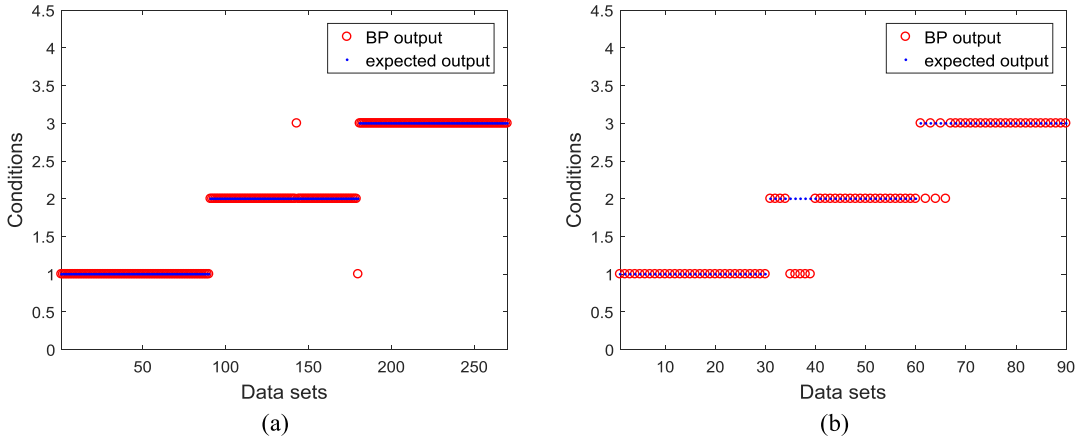

FIGURE 18. BP neural network results by utilizing 7 orders IMFs of APIT-MEMD and MMSE: (a) Training sets, (b) Testing sets.

TABLE 3. The output layer neurons of BP neural network.

Fault types	Neural nodes
Inner race defect	[1 0 0]
Ball defect	[0 1 0]
Outer race defect	[0 0 1]

be taken as effective condition indicators in fault diagnosis of rolling bearings. Thus, the proposed approach with processing multivariate signals is conducted to achieve fault classification of rolling bearings. To explore the appropriate order of the adopted IMFs and use IMMSE of them as input values of BP neural network, the first 4 orders IMFs are adopted in the proposed approach as a trial. The results of neural network adopting IMMSE of the first 4 orders IMFs, obtained by APIT-MEMD-AN of multivariate signals of faulty rolling bearings under varying operating conditions, are shown in Fig. 16.

Fig. 16 shows that fault classification accuracies of testing sets are not good. The inner race defect of rolling bearings is classified accurately, and ball and outer race defects of rolling bearings are not classified properly. Fault classification accuracies of ball and outer race defects of rolling bearings in testing process of BP neural network are 66.7% and 80%, respectively. The unsatisfactory results are most likely caused by insufficient orders IMFs adopted for IMMSE, namely insufficient effective input values of BP neural network. The reason of bad performance of fault classification of rolling bearings here is that insufficient orders IMFs do not contain enough dynamical response information of different kinds of faulty rolling bearings. After the trial of adopting the first 4 orders IMFs, multiple experiments are conducted adopting different numbers of IMFs afterwards. The first 7 orders IMFs are determined as optimal orders for IMMSE computing after repeated experimental validation and regarded as proper input values of BP neural network.

To verify the superiority of the proposed approach in this paper, comparisons of approaches adopting similar strategies are given here. The results of BP neural network adopting IMMSE of the first 7 orders IMFs, obtained by MEMD of multivariate signals, are shown in Fig. 17. The results of BP neural network adopting MMSE of the first 7 orders IMFs, obtained by APIT-MEMD of multivariate signals, are shown in Fig. 18. The results of BP neural network adopting IMMSE of the first 7 orders IMFs, obtained by APIT-MEMD of multivariate signals, are shown in Fig. 19.

Fig. 17, Fig. 18 and Fig. 19 show that the abovementioned approaches adopting similar strategies to multivariate intrinsic multiscale entropy analysis and BP neural network achieve different effects in fault diagnosis results of rolling bearings under varying operating conditions. In Fig. 17, Fig. 18 and Fig. 19, fault classification accuracies of inner race defect of rolling bearings in testing process of BP neural network are 100%. Fig. 17 shows that fault classification accuracies of ball and outer race defects of rolling bearings in testing process of BP neural network are 83.3% and 90%, respectively. Fig. 18 shows that fault classification accuracies of ball and outer race defects of rolling bearings in testing process of BP neural network are 83.3% and 90%, respectively. Fig. 19 shows that fault classification accuracies of ball and outer race defects of rolling bearings in testing process of BP neural network are respectively 93.3% and 90%. The comparative analysis of classification results between Fig. 17 and Fig. 19 verifies the superiority of APIT-MEMD. The comparative analysis of classification results between Fig. 18 and Fig. 19 illustrates the superiority of the proposed IMMSE. The above analysis of classification results verifies the superiority of APIT-MEMD and IMMSE. The above analysis illustrates that the proposed strategy in this paper is effective in classifying different kinds of defects of rolling bearings under varying operating conditions.

The proposed fault diagnosis approach of rolling bearings under varying operating conditions in this paper employs multivariate intrinsic multiscale entropy analysis consisting

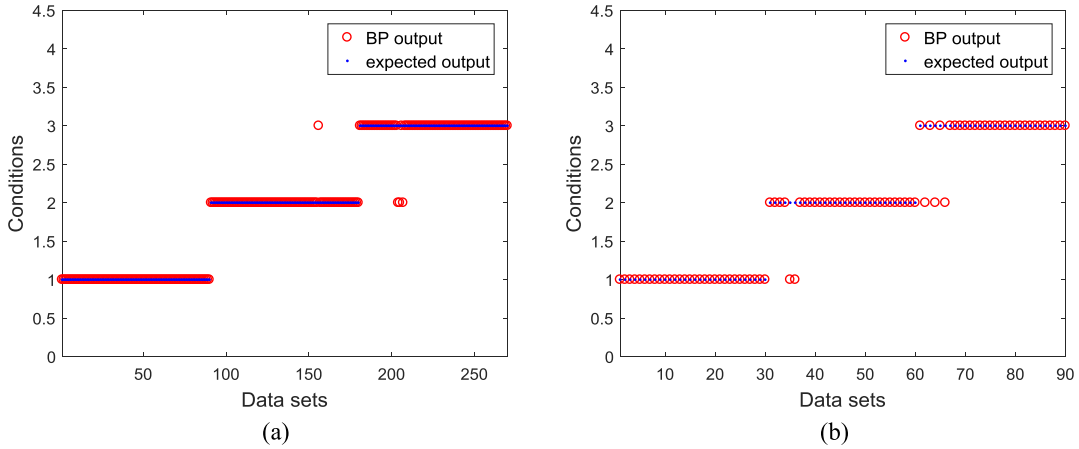

FIGURE 19. BP neural network results by utilizing 7 orders IMFs of APIT-MEMD and IMMSE: (a) Training sets, (b) Testing sets.

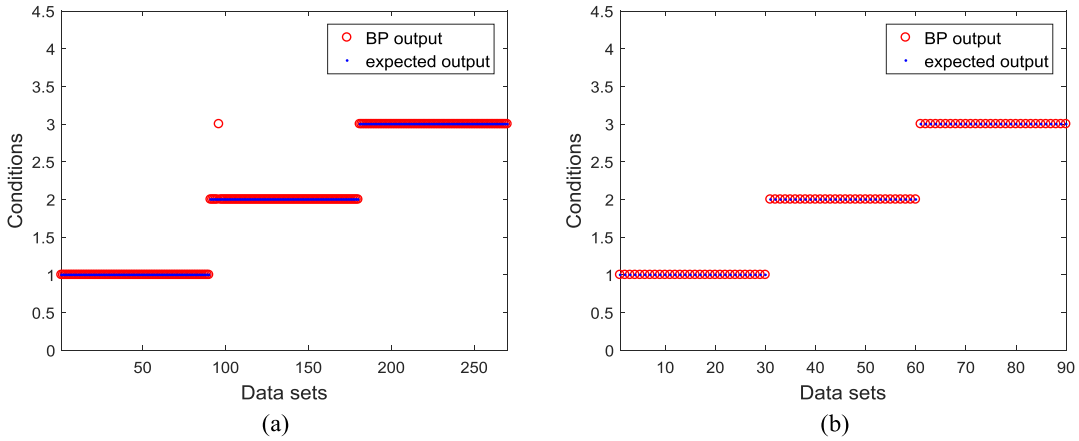

FIGURE 20. BP neural network results by utilizing 7 orders IMFs of APIT-MEMD-AN and IMMSE: (a) Training sets, (b) Testing sets.

of APIT-MEMD-AN and IMMSE, combined with BP neural network. The results of BP neural network adopting IMMSE values of the first 7 orders IMFs, obtained by APIT-MEMD-AN of multivariate signals, are shown in Fig. 20.

Fig. 20 shows that the proposed approach using multivariate intrinsic multiscale entropy analysis consisting of APIT-MEMD-AN and IMMSE, combined with BP neural network achieves perfect fault diagnosis results. Fault classification accuracies of inner race, ball and outer race defects of rolling bearings in testing processing of BP neural network are 100%. The comparative analysis of classification results between Fig. 19 and Fig. 20 illustrates the superiority of the proposed APIT-MEMD-AN. Classification results indicate that the proposed approach using APIT-MEMD-AN and IMMSE achieves optimal fault diagnosis results.

The above analysis shows the effectiveness and superiority of our proposed approach. Further, to verify the superiority of the proposed approach, 30 times of experiments employing abovementioned strategies are conducted to get the averages of fault classification accuracies. The results of BP neural network of fault classification accuracies adopting different strategies are shown in Table 4.

TABLE 4. The fault classification accuracies of rolling bearings of the results of BP neural network under varying operating conditions using different strategies (adopting 7 orders IMFs).

Defect types / Strategies	Inner race defect	Ball	Outer race defect
EMD+SE	82.57%	71.33%	76.67%
MEMD+IMMSE	100%	82.78%	91.47%
APIT-MEMD+MMSE	100%	84.97%	90.18%
APIT-MEMD+IMMSE	100%	93.65%	92.73%
APIT-MEMD-AN+IMMSE	100%	99.34%	99.67%

It can be seen from the Table 4 that the proposed approach achieves best classification accuracies compared to strategies adopting other methods involving APIT-MEMD and MMSE. The results validate the superiority of our proposed novel methods: APIT-MEMD-AN, IMMSE and the

proposed approach of fault diagnosis under varying operating conditions.

VI. DISCUSSION AND CONCLUSION

The proposed robust fault diagnosis approach provides a novel approach to achieve fault diagnosis of rotary machinery under varying operating conditions. Multivariate intrinsic multiscale entropy analysis consists of APIT-MEMD-AN and IMMSE. APIT-MEMD-AN has fully data driven intrinsic characteristic and IMMSE has the underlying robust characteristic, making the proposed approach a fully data driven and robust approach. Multivariate signals are decomposed by APIT-MEMD-AN to get multiple sets of IMFs, and IMMSE of certain IMFs are adopted as input values of BP neural network to achieve fault diagnosis of rolling bearings. The validity and superiority of the proposed approach are verified by theoretical derivations, numerical simulations and experimental verification. The research work demonstrates that the proposed approach is promising in fault diagnosis of rolling bearing under varying operating conditions. In future work, multivariate intrinsic multiscale entropy analysis combined with neural network will be adopted in related fields of structural health monitoring, and other new fields. Different classifiers will be considered to assist multivariate intrinsic multiscale entropy analysis in extracting dynamical properties of different kinds of systems. The major findings of the proposed approach are summarized as follows:

1) The way of processing multivariate signals caters to the fast and wide developments of multi-sensor acquisition system. By using multiple sensors to collect multivariate signals of rolling bearings, it captures more dynamical information than single sensor. Inaccurate results of fault diagnosis are avoided by cross-information between multiple channels.
2) MEMD-derived methods have advantages, including mode alignment across multiple channels, adaptive arrangement of high-to-low instantaneous frequencies, same locations of characteristic frequencies in IMFs. Further, APIT-MEMD and APIT-MEMD-AN alleviate adverse effect of power imbalances among multiple channels by adaptive projection vectors. In addition, APIT-MEMD-AN has two advantages against APIT-MEMD. It utilizes filter bank property in the presence of Gaussian white noise with frequency uniformly distribution property to alleviate mode mixing problem. By adding specific noise to each residue in each iteration to obtain one IMF set each time, the same amounts of IMFs are obtained under different ensemble times, which benefits for subsequent analysis of adopting certain orders IMFs.
3) The proposed IMMSE algorithm measures the complexity and regularity of multivariate vibration signals of faulty rolling bearings. The proposed smoothed coarse graining process improves MMSE algorithm. IMMSE measures intrinsic properties of multivariate signals instead of energy or frequency amplitudes, and it won't be affected by defect diameter, motor load or speed, which endows the proposed approach with the intrinsic robustness. Hence the proposed approach can be well applied in the fault diagnosis of rolling bearings under varying operating conditions.
4) The actual output of BP neural network is consistent with the theoretical output during the training and testing process of the proposed approach. It has the advantage of simple network structure and convenient parameter adjustment. The results demonstrate that BP neural network can be effectively adopted to fault diagnosis of rolling bearings. It helps to demonstrate the effectiveness and superiority of multivariate intrinsic multiscale entropy analysis proposed in this paper.

REFERENCES

[1] R. B. Randall and J. Antoni, "Rolling element bearing diagnostics—A tutorial," *Mech. Syst. Signal Process.*, vol. 25, no. 2, pp. 485–520, Feb. 2011.
[2] H. R. Cao, L. Niu, S. Xi, and X. Chen, "Mechanical model development of rolling bearing-rotor systems: A review," *Mech. Syst. Signal. Process.*, vol. 102, pp. 37–58, Mar. 2018.
[3] B. Yao, P. Zhen, L. Wu, and Y. Guan, "Rolling element bearing fault diagnosis using improved manifold learning," *IEEE Access*, vol. 5, pp. 6027–6035, 2017.
[4] Z. Huo, Y. Zhang, P. Francq, L. Shu, and J. Huang, "Incipient fault diagnosis of roller bearing using optimized wavelet transform based multi-speed vibration signatures," *IEEE Access*, vol. 5, pp. 19442–19456, 2017.
[5] S.-H. Wang, T.-M. Zhan, Y. Chen, Y. Zhang, M. Yang, H.-M. Liu, H.-N. Wang, B. Liu, P. Phillips, "Multiple sclerosis detection based on biorthogonal wavelet transform, RBF kernel principal component analysis, and logistic regression," *IEEE Access*, vol. 4, pp. 7567–7576, 2016.
[6] H. Darong, K. Lanyan, M. Bo, Z. Ling, and S. Guoxi, "A new incipient fault diagnosis method combining improved RLS and LMD algorithm for rolling bearings with strong background noise," *IEEE ACCESS*, vol. 6, pp. 26001–26010, 2018.
[7] X. Lang, P. Li, Z. Hu, H. Ren, and Y. Li, "Leak detection and location of pipelines based on LMD and least squares twin support vector machine," *IEEE Access*, vol. 5, pp. 8659–8668, 2017.
[8] Y. Wang, R. Markert, J. Xiang, and W. Zheng, "Research on variational mode decomposition and its application in detecting rub-impact fault of the rotor system," *Mech. Syst. Signal Process.*, vols. 60–61, pp. 243–251, Aug. 2015.
[9] F. Jiang, Z. Zhu, and W. Li, "An improved VMD with empirical mode decomposition and its application in incipient fault detection of rolling bearing," *IEEE Access*, vol. 6, pp. 44483–44493, 2018.
[10] Y. Lei, J. Lin, Z. He, and M. J. Zuo, "A review on empirical mode decomposition in fault diagnosis of rotating machinery," *Mech. Syst. Signal Process.*, vol. 35, nos. 1–2, pp. 108–126, Feb. 2013.
[11] S. Park, S. Kim, and J.-H. Choi, "Gear fault diagnosis using transmission error and ensemble empirical mode decomposition," *Mech. Syst. Signal Process.*, vol. 108, pp. 262–275, Aug. 2018.
[12] X. Yu, F. Dong, E. Ding, S. Wu, and C. Fan, "Rolling bearing fault diagnosis using modified LFDA and EMD with sensitive feature selection," *IEEE Access*, vol. 6, pp. 3715–3730, 2017.
[13] T. Tanaka and D. P. Mandic, "Complex empirical mode decomposition," *IEEE Signal Process. Lett.*, vol. 14, no. 2, pp. 101–104, Feb. 2007.
[14] M. U. B. Altaf, T. Gautama, T. Tanaka, and D. P. Mandic, "Rotation invariant complex empirical mode decomposition," in *Proc. IEEE ICASSP*, Apr. 2007, pp. 1009–1012.
[15] T. Wang, G. Lu, and P. Yan, "Multi-sensors based condition monitoring of rotary machines: An approach of multidimensional time-series analysis," *Measurement*, vol. 134, pp. 326–335, Feb. 2019.
[16] P. W. Tse, S. Gontarz, and X. J. Wang, "Enhanced eigenvector algorithm for recovering multiple sources of vibration signals in machine fault diagnosis," *Mech. Syst. Signal. Process.*, vol. 21, no. 7, pp. 2794–2813, Oct. 2007.

[17] G. Rilling, P. Flandrin, P. Goncalves, and J. M. Lilly, "Bivariate empirical mode decomposition," *IEEE Signal Process. Lett.*, vol. 14, no. 12, pp. 936–939, Dec. 2007.
[18] W. Yang, R. Court, P. J. Tavner, and C. J. Crabtreeb, "Bivariate empirical mode decomposition and its contribution to wind turbine condition monitoring," *J. Sound Vib.*, vol. 330, no. 15, pp. 3766–3782, Jul. 2011.
[19] A. Ahrabian, N. U. Rehman, and D. Mandic, "Bivariate empirical mode decomposition for unbalanced real-world signals," *IEEE Signal Process. Lett.*, vol. 20, no. 3, pp. 245–248, Mar. 2013.
[20] N. U. Rehman and D. P. Mandic, "Empirical mode decomposition for trivariate signals," *IEEE Trans. Signal Process.*, vol. 58, no. 3, pp. 1059–1068, Mar. 2010.
[21] N. U. Rehman and D. P. Mandic, "Multivariate empirical mode decomposition," *Proc. R. Soc. Lond. A, Math., Phys. Eng. Sci.*, vol. 466, no. 2117, pp. 1291–1302, Dec. 2009.
[22] J. Fleureau, A. Kachenoura, L. Albera, J. C. Nunes, and L. Senhadji, "Multivariate empirical mode decomposition and application to multichannel filtering," *Signal Process.*, vol. 91, no. 12, pp. 2783–2792, Dec. 2011.
[23] X. Zhao, T. H. Patel, and M. J. Zuo, "Multivariate EMD and full spectrum based condition monitoring for rotating machinery," *Mech. Syst. Signal. Process.*, vol. 27, pp. 712–728, Feb. 2012.
[24] J. Kim, S.-K. Lee, and B. Lee, "EEG classification in a single-trial basis for vowel speech perception using multivariate empirical mode decomposition," *J. Neural Eng.*, vol. 11, no. 3, May 2014, Art. no. 036010.
[25] J. B. Sharma, K. K. Sharma, and V. Sahula, "Hybrid image fusion scheme using self-fractional Fourier functions and multivariate empirical mode decomposition," *Signal Process.*, vol. 100, pp. 146–159, Jul. 2014.
[26] M. E. Torres, M. A. Colominas, G. Schlotthauer, and P. Flandrin, "A complete ensemble empirical mode decomposition with adaptive noise," in *Proc. IEEE ICASSP*, May 2011, pp. 4144–4147.
[27] Y. Xu, M. Luo, T. Li, and G. Song, "ECG signal de-noising and baseline wander correction based on CEEMDAN and wavelet threshold," *Sensors*, vol. 17, no. 12, p. 2754, Nov. 2017.
[28] N. U. Rehman and D. P. Mandic, "Filter bank property of multivariate empirical mode decomposition," *IEEE Trans. Signal Process.*, vol. 59, no. 5, pp. 2421–2426, May 2011.
[29] M. S. Koh and E. Rodriguez-Marek, "Perfect reconstructable decimated two-dimensional empirical mode decomposition filter banks," *J. Electron. Sci. Techn.*, vol. 12, no. 2, pp. 196–200, May 2013.
[30] M. S. Koh, D. P. Mandic, and A. G. Constantinides, "Theory of digital filter banks realized via multivariate empirical mode decomposition," *Adv. Adapt. Data Anal.*, vol. 6, no. 1, Jan. 2014, Art. no. 1450001.
[31] N. U. Rehman, M. W. Safdar, U. U. Rehman, and D. P. Mandic, "Dynamically-sampled bivariate empirical mode decomposition," *IEEE Signal Process. Lett.*, vol. 21, no. 7, pp. 857–861, Jul. 2014.
[32] A. Hemakom, A. Ahrabian, D. Looney, N. U. Rehman, and D. P. Mandic, "Nonuniformly Sampled Trivariate Empirical Mode Decomposition," in *Proc. IEEE ICASSP*, Apr. 2015, pp. 3691–3695.
[33] A. Hemakom, V. Goverdovsky, D. Looney, and D. P. Mandic, "Adaptive-projection intrinsically transformed multivariate empirical mode decomposition in cooperative brain–computer interface applications," *Philos. Trans. Roy. Soc. A, Math., Phys. Eng. Sci.*, vol. 374, no. 2065, Apr. 2016, Art. no. 20150199.
[34] S. M. Pincus, "Approximate entropy as a measure of system complexity," *Proc. Nat. Acad. Sci. USA*, vol. 88, pp. 2297–2301, Mar. 1991.
[35] J. S. Richman and M. J. Randall, "Physiological time-series analysis using approximate entropy and sample entropy," *Amer. J. Physiol.-Heart Circulatory Physiol.*, vol. 278, no. 6, pp. H2039–H2049, Jul. 2000.
[36] J. M. Yentes, N. Hunt, K. K. Schmid, J. P. Kaipust, D. McGrath, and N. Stergiou, "The appropriate use of approximate entropy and sample entropy with short data sets," *Ann. Biomed. Eng.*, vol. 41, no. 2, pp. 349–365, Feb. 2013.
[37] M. Costa, A. L. Goldberger, and C.-K. Peng, "Multiscale entropy analysis of complex physiologic time series," *Phys. Rev. Lett.*, vol. 89, no. 6, pp. 705–708, Sep. 2002.
[38] X. Zhang, X. Chen, P. E. Barkhaus, and P. Zhou, "Multiscale entropy analysis of different spontaneous motor unit discharge patterns," *IEEE J. Biomed. Health Informat.*, vol. 17, no. 2, pp. 470–476, Mar. 2013.
[39] Y. Y. Wu, Y. Chen, Y. Yu, T. Yan, and R. Song, "Age-related differences in complexity during handgrip control using multiscale entropy," *IEEE Access*, vol. 6, pp. 45552–45561, 2018.
[40] Y. Li, X. Wang, Z. Liu, X. Liang, and S. Si, "The entropy algorithm and its variants in the fault diagnosis of rotating machinery: A review," *IEEE Access*, vol. 6, pp. 66723–66741, 2018.
[41] Q. W. Gao, W. Y. Liu, B. P. Tang, and G. J. Li, "A novel wind turbine fault diagnosis method based on intergral extension load mean decomposition multiscale entropy and least squares support vector machine," *Renew. Energ.*, vol. 116, pp. 169–175, Feb. 2018.
[42] M. U. Ahmed and D. P. Mandic, "Multivariate multiscale entropy: A tool for complexity analysis of multichannel data," *Phys. Rev. E, Stat. Phys. Plasmas Fluids Relat. Interdiscip. Top.*, vol. 84, no. 6, Dec. 2011, Art. no. 061918.
[43] M. U. Ahmed and D. P. Mandic, "Multivariate multiscale entropy analysis," *IEEE Signal Process. Lett.*, vol. 19, no. 2, pp. 91–94, Feb. 2012.
[44] M. U. Ahmed, L. Li, J. Cao, and P. M. Danilo, "Multivariate multiscale entropy for brain consciousness analysis," in *Proc. 33rd EMBS*, Aug. 2011, pp. 810–813.
[45] Z.-K. Gao, M.-S. Ding, H. Geng, and N.-D. Jin, "Multivariate multiscale entropy analysis of horizontal oil–water two-phase flow," *Phys. A, Statist. Mech. Appl.*, vol. 417, pp. 7–17, Jan. 2015.
[46] Y. Lv, R. Yuan, T. Wang, H. Li, and G. Song, "Health degradation monitoring and early fault diagnosis of a rolling bearing based on CEEMDAN and improved MMSE," *Materials*, vol. 11, no. 6, p. 1009, Jun. 2018.
[47] Y. Lv, R. Yuan, and G. Song, "Multivariate empirical mode decomposition and its application to fault diagnosis of rolling bearing," *Mech. Syst. Signal Process.*, vol. 81, pp. 219–234, Dec. 2016.
[48] R. Yuan, Y. Lv, and G. Song, "Multi-fault diagnosis of rolling bearings via adaptive projection intrinsically transformed multivariate empirical mode decomposition and high order singular value decomposition," *Sensors*, vol. 18, no. 4, p. 1210, Apr. 2018.
[49] G. F. Wang, Y. B. Li, and Z. G. Luo, "Fault classification of rolling bearing based on reconstructed phase space and Gaussian mixture model," *J. Sound Vib.*, vol. 323, nos. 3–5, pp. 1077–1089, Jun. 2009.
[50] S. P. Garcia and J. S. Almeida, "Nearest neighbor embedding with different time delays," *Phys. Rev. E, Stat. Phys. Plasmas Fluids Relat. Interdiscip. Top.*, vol. 72, no. 2, Aug. 2005, Art. no. 027205.
[51] D. Looney, A. Hemakom, and D. Mandic, "Intrinsic multi-scale analysis: A multi-variate empirical mode decomposition framework," *Proc. Math. Phys. Eng. Sci.*, vol. 471, no. 2173, p. 20140709, Jan. 2015.
[52] R. Ricci and P. Pennacchi, "Diagnostics of gear faults based on emd and automatic selection of intrinsic mode functions," *Mech. Syst. Signal. Process.*, vol. 25, no. 3, pp. 821–838, Apr. 2011.
[53] M. Hu and H. Liang, "Intrinsic mode entropy based on multivariate empirical mode decomposition and its application to neural data analysis," *Cogn. Neurodyn.*, vol. 5, no. 3, pp. 277–284, Sep. 2011.
[54] B. Jatin and D. Toshniwal, "Empirical mode decomposition based deep learning for electricity demand forecasting," *IEEE Access*, vol. 6, pp. 49144–49156, 2018.
[55] S. Liu, Y. Sun, and L. Zhang, "A novel fault diagnosis method based on noise-assisted MEMD and functional neural fuzzy network for rolling element bearings," *IEEE Access*, vol. 6, pp. 27048–27068, 2018.
[56] Y. Qi, C. Shen, D. Wang, J. Shi, X. Jiang, and Z. Zhu, "Stacked sparse autoencoder-based deep network for fault diagnosis of rotating machinery," *IEEE Access*, vol. 5, pp. 15066–15079, 2017.
[57] R. Zhang, H. Tao, L. Wu, and Y. Guan, "Transfer learning with neural networks for bearing fault diagnosis in changing working conditions," *IEEE Access*, vol. 5, pp. 14347–14357, 2017.
[58] W. A. Smith and R. B. Randall, "Rolling element bearing diagnostics using the Case Western Reserve University data: A benchmark study," *Mech. Syst. Signal Process.*, vols. 64–65, pp. 100–131, Dec. 2015.

RUI YUAN received the B.S. degree in mechanical engineering from the Department of Mechanical Engineering, Wuhan University of Science and Technology, Wuhan, China, in 2014, where he is currently pursuing the Ph.D. degree in mechanical engineering. From 2016 to 2017, he was a Visiting Scholar with the Nonlinear Dynamics Laboratory, University of Rhode Island, Kingston, RI, USA. He has published over six peer-reviewed journals, including MSSP, SMS, *Complexity*, and *Materials*. His current research interests include fault detection and isolation, prognostics and health management, structural health monitoring, and nonlinear dynamics. He received the National Award for Distinguished Doctorates and Postgraduate Overseas Visiting Scholar Funding from the Wuhan University of Science and Technology.

YONG LV received the B.S. and M.S. degrees from the Department of Mechanical Engineering, Wuhan University of Science and Technology, Wuhan, China, in 1998 and 2000, respectively, and the Ph.D. degree from the University of Science and Technology Beijing, Beijing, China, in 2004. He is currently a Full Professor with the School of Machinery and Automation, Wuhan University of Science and Technology. He has published over 100 peer-reviewed journals, including MSSP, *Measurement*, and *Spectrochimica Acta B*. He has hosted three National Natural Science Foundations of China. He has hosted over 30 projects in the field of machinery dynamics and condition monitoring. His current research interests include fault detection and isolation, prognostics and health management, structural health monitoring, and nonlinear dynamics.

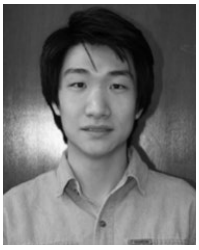

HEWENXUAN LI received the B.S. degree from the Department of Vehicle Engineering, Beijing Forestry University, Beijing, China, in 2016. He is currently pursuing the Ph.D. degree in mechanical engineering and engineering mechanics with the University of Rhode Island. Since the beginning of the Ph.D. study, he was a Research Assistant with Nonlinear Dynamics Laboratory under the supervision of Prof. D. Chelidze. His major concentration of study focus on statistics driven fatigue life prediction under variable amplitude loading. His current research interests include but are not limited to structural health monitoring, nonlinear system identification, nonlinear vibration, and data-driven modeling. He received the Enhancement of Graduate Research Award from the University of Rhode Island, in 2018.

GANGBING SONG received the B.S. degree from Zhejiang University, China, in 1989, and the M.S. and Ph.D. degrees from the Department of Mechanical Engineering, Columbia University, New York, NY, USA, in 1991 and 1995, respectively. He is currently the Founding Director of the Smart Materials and Structures Laboratory and a Professor of mechanical engineering, civil and environmental engineering, and electrical and computer engineering with the University of Houston. He has developed two new courses in smart materials and published over 400 articles, including 196 peer-reviewed journal articles. His current research interests include smart materials and structures, structural vibration control, piezoceramics, ultrasonic transducers, structural health monitoring, and damage detection. He was a recipient of the NSF CAREER Award, in 2001.